Title

Understanding the influence of disorder on the exciton dynamics and energy transfer in Zn-phthalocyanine H-aggregates

Journal

Physical Chemistry Chemical Physics, 20(34)

ISSN

0956-5000

Authors

Doria, Sandra
Lapini, Andrea
Di Donato, Mariangela
et al.

Publication Date

2018-08-29

DOI

10.1039/c8cp02172d

Peer reviewed

PCCP

PAPER

View Article Online
View Journal

Cite this: DOI: 10.1039/c8cp02172d

Understanding the influence of disorder on the exciton dynamics and energy transfer in Zn-phthalocyanine H-aggregates†

Sandra Doria, [ab] Andrea Lapini, *[ab] Mariangela Di Donato, [ac] Roberto Righini, [ab] Nicolò Azzaroli, [a] Alessandro Iagatti, [ac] Justin R. Caram, [d] Timothy S. Sinclair, [e] Lorenzo Cupellini, [f] Sandro Jurinovich, [f] Benedetta Mennucci, [f] Gloria Zanotti, [g] Anna Maria Paoletti, [g] Giovanna Pennesi [g] and Paolo Foggi [achi]

The photophysics of 9(19),16(17),23(24)-tri-*tert*-butyl-2-[ethynyl-(4-carboxymethyl)phenyl]phthalocyaninatozinc(II) and its H-aggregates is studied in different solvents by means of ultrafast non-linear optical spectroscopy and computational modeling. In non-coordinating solvents, both stationary and time-resolved spectroscopies highlight the formation of extended molecular aggregates, whose dimension and spectral properties depends on the concentration. In all the explored experimental conditions, time-resolved transient absorption experiments show multi exponential decay of the signals. Additional insights into the excited state relaxation mechanisms of the system is obtained with 2D electronic spectroscopy, which is employed to compare the deactivation channels in the absence or presence of aggregates. In ethanol and diethylether, where only monomers are present, an ultrafast relaxation process among the two non-degenerate Q-states of the molecule is evidenced by the appearance of a cross peak in the 2D-maps. In chloroform or CCl_4, where disordered H-aggregates are formed, an energy transfer channel among aggregates with different composition and size is observed, leading to the non-radiative decay towards the lower energy dark state of the aggregates. Efficient coupling between less and more aggregated species is highlighted in two-dimensional electronic spectra by the appearance of a cross peak. The kinetics and intensity of the latter depend on the concentration of the solution. Finally, the linear spectroscopic properties of the aggregate are reproduced using a simplified structural model of an extended aggregate, based on Frenkel Hamiltonian Calculations and on an estimate of the electronic couplings between each dimer composing the aggregate computed at DFT level.

Received 5th April 2018,
Accepted 3rd August 2018

DOI: 10.1039/c8cp02172d

rsc.li/pccp

Introduction

Phthalocyanine-based materials have received increased attention due to their versatility and potential employment in many applications.[1,2] Such molecules represent an alternative to porphyrins and perylene, displaying higher chemical and thermal stability while maintaining analogous electronic properties.[1,3–5] Phthalocyanine dyes indeed possess elevated fluorescence quantum yield (QY), intense absorption cross-section in a wide spectral region and anisotropic electrical and optical properties, features that make them suitable for acting as light-harvesting material in Dye Sensitized Solar Cells (DSSCs),[6–9] inorganic solar-cell junctions, as well as for the fabrication of electroluminescent devices.[10] Due to their extended π aromatic structures, these molecules have large third-order susceptibility and can be used for the development of non-linear optic devices.[11,12] Furthermore, the presence of long-lived triplet states,[13,14] the high catalytic activity[15,16] and the ability to produce singlet oxygen have applications in photodynamic therapies (PDT) for cancer treatment.[17–19]

[a] European Laboratory for Non Linear Spectroscopy (LENS), Università degli Studi di Firenze, via Nello Carrara 1, 50019 Sesto Fiorentino, Florence, Italy. E-mail: lapini@lens.unifi.it
[b] Dipartimento di Chimica "Ugo Schiff", Università degli Studi di Firenze, via della Lastruccia, 3-13, 50019 Sesto Fiorentino, Florence, Italy
[c] CNR-INO, Consiglio Nazionale delle Ricerche – Istituto Nazionale di Ottica, Largo Fermi 6, 50125 Florence, Italy
[d] Chemistry and Biochemistry Department, UCLA, 607 Charles E. Young Drive East, Los Angeles, CA 90095-1569, USA
[e] Department of Chemistry, Massachusetts Institute of Technology, Cambridge, Massachusetts 02139, USA
[f] Dipartimento di Chimica e Chimica Industriale, Università di Pisa, via G. Moruzzi 13, 56124, Pisa, Italy
[g] CNR-ISM, Consiglio Nazionale delle Ricerche-Istituto Struttura della Materia, via Salaria Km. 29.5, 00015 Monterotondo Stazione, Roma, Italy
[h] Dipartimento di Chimica, Biologia e Biotecnologie, Università di Perugia, via Elce di Sotto 8, 06100 Perugia, Italy
[i] CNR-ICCOM, Consiglio Nazionale delle Ricerche-Istituto-Istituto di Chimica dei Composti OrganoMetallici, via Madonna del Piano 10, 50019 Sesto Fiorentino, Firenze, Italy

† Electronic supplementary information (ESI) available. See DOI: 10.1039/c8cp02172d

A main advantage of phthalocyanines is the chemical tunability of their electronic and non-linear optic properties. It has been demonstrated that changing the central atom or introducing peripheral substituents modify the electronic distribution, influencing the electron delocalization and the exciton coupling in condensed phases.[20,21] Functionalization of these molecules thus opens a wide range of possibilities in engineering of artificial systems with specifically tailored properties.

Structural modifications of phthalocyanines are required to increase their solubility and to prevent aggregation, especially in water due to hydrophobic interactions.[20,22] Increased solubility in organic solvents is mostly achieved through chemical modifications, such as addition of long side chains.[23,24] Aggregation and low solubility are responsible for fluorescence quantum yield (QY) depletion, and represent a negative issue both for drug delivery and for PDT applications, because of a lower efficiency in singlet oxygen generation. In addition, aggregation limits the use of these systems in the photo-voltaic field.[25] However, self-assembling of phthalocyanines in ordered supramolecular structures may represent an advantage rather than a disadvantage in several specific cases. For example, even if standard phthalocyanines express mesomorphic behavior, aggregate forms can show directional exciton delocalization, with increased absorption dipole moments enabling increased electron–hole transfer. Previous studies show the possibility of creating charge carriers migrating along molecular organized paths, enhancing the conducting properties of aggregate based materials.[23,26] Thin layers made of phthalocyanines have shown to possess long-range order and high rigidity.[27–29]

In this work, we explore the aggregation phenomenon occurring in a substituted Zn-phthalocyanine (9(19),16(17),23(24)-tri-*tert*-butyl-2-[ethynyl-(4-carboxymethyl)phenyl]phthalocyaninato-zinc(II) = ZnPc) dye through stationary and time-resolved coherent multidimensional spectroscopic techniques. Linear absorption and emission highlight the presence of supramolecular structures dominated by non-fluorescent H-type aggregates. The nature of aggregation is studied in different solvents and supported by a TEM investigation, which shows the presence of fibrous assemblies. A deeper characterization of the electronic properties of these aggregates is achieved by ultrafast broadband pump–probe and 2D Electronic Spectroscopy (2DES), which is able to identify the correlation between different molecular assemblies and to highlight the electronic coupling between the excited states of more aggregated and less aggregated (or monomer) species in solution.

Finally, Density Functional Theory (DFT) calculations are employed to reproduce the electronic properties of the monomer in different solvents and to estimate the electronic structure of the simpler multichromophore structure, namely a dimeric structure. High accurate *ab initio* calculations are in fact still challenging for multichromophoric systems with large sizes, making prohibitive to investigate the electronic and geometrical properties of more extended aggregate systems at the DFT level. For this reason, we utilize a Frenkel exciton Hamiltonian using a simplified structural model to simulate the aggregate linear spectral properties.[30,31] This approach allows us to reproduces the absorption spectrum of the system in the presence of extended H-aggregates to give an estimate of the exciton delocalization extent.

Materials and methods

The synthesis and structural characterization of ZnPc dye under investigation (molecular structure in Fig. 1a) was reported in a previous publication.[29] Linear absorption and emission data were recorded using a Perkin Elmer Lambda950 spectrometer and a Perkin Elmer LS55 fluorimeter. TEM measurements were performed using a TEM CM 12 Philips instrument.

2DES measurements were performed with the setup presented in Fig. S1 of ESI† and previously described.[32] Ultrafast pulses were generated by a self-mode locking Ti:Sapphire oscillator (Coherent Micra) producing 810 nm, 85 nm bandwidth (400 mW, 89 MHz) pulses. The pulses are amplified using a Coherent Legend Elite system, generating ultrafast pulses at 800 nm, which are compressed to 35 fs duration (3 mJ per pulse, 1 kHz). A detailed description of the 2DES setup is reported in ESI.† A homemade Non-Collinear Optical Parametric Amplifier (NOPA)[51] can be tuned to emit broadband pulses in the green-red region of the spectrum (details can be found elsewhere).[52] Three out of the four beams in the box-CAR geometry induce the third order polarization signal in the sample, which is emitted in the direction of the fourth beam (local oscillator), allowing for hetherodyne detection. Echo and local oscillator interfere onto the detector after passing a spectrometer. The entire acquisition system, including electronics for read-out of the arrays, signal amplification, data digitalization and treatment is homemade. By switching the time ordering between the two pump beams, rephasing and non-rephasing maps are collected. Fourier transforming along their time delays yields the excitation frequency axes. The absorptive 2D spectra are obtained summing the real part of rephasing and non-rephasing signals, after the phasing procedure and data treatment are performed as described in ESI.† Broadband transient absorption measurements are carried out on the same setup, allowing the phasing procedure to be done following the projection theorem.

Calculations on monomeric ZnPc were performed employing DFT and its time-dependent formulation for excited-state properties. Geometry optimizations were carried out at the B3LYP/6-31G(d) level of theory. Excited state calculations were carried out with the M06-2X functional[33] and the 6-31+G(d) basis set, systematically including the solvent effect with the IEFPCM[34] method. Test calculations with different functionals gave correct solvatochromic shifts. In order to estimate the structure of dimeric aggregates, we started from several guess cofacial dimers with different orientations. These structures were fully optimized at the B3LYP/6-311G(d) level with Grimme's empirical dispersion correction.[35] The most stable dimer structures were selected for excitonic calculations. Exciton couplings were determined as the interaction between the quantum-mechanical transition densities of the interacting monomers.[36] The same couplings were also computed employing the

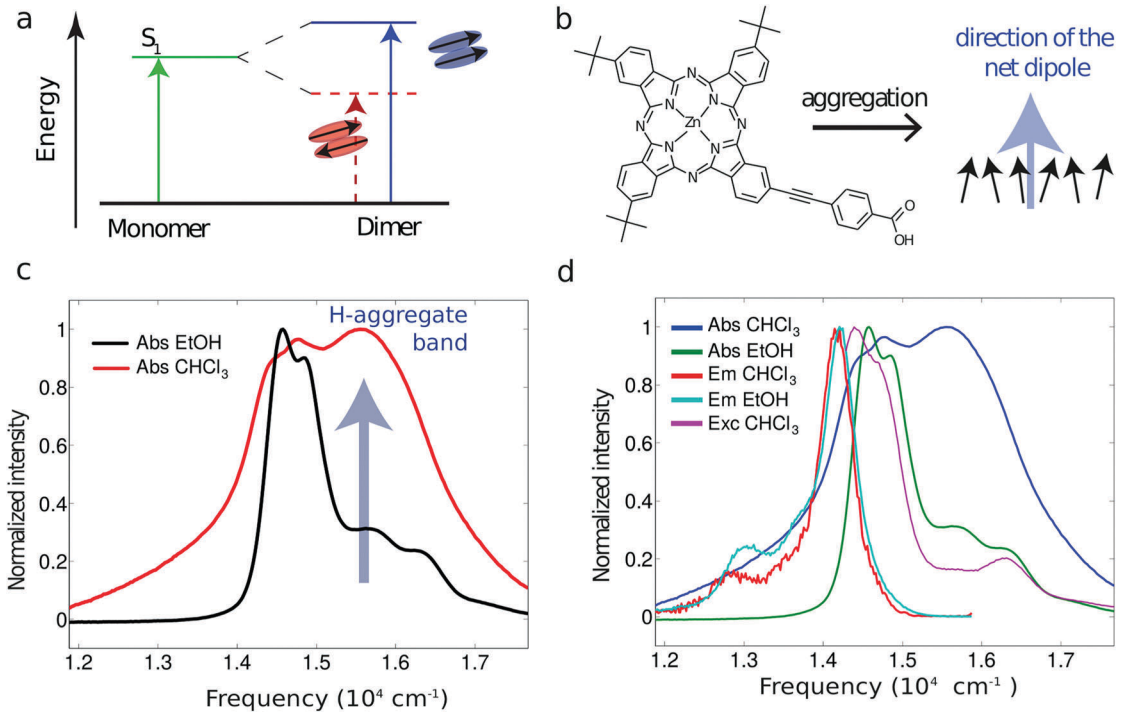

Fig. 1 (a) Schematic representation of the energy level splitting going from an isolated monomer to a coupled dimer. Two transitions have different dipole strength depending on the monomer arrangement, and only the high energy transition is allowed in case of the sandwich geometry (H-aggregates). (b) Chemical structure of the ZnPc dye molecule and schematic representation of dipole moments orientation typical of H-aggregates. (c) Absorption spectra of the substituted ZnPc dye in ethanol and in chloroform solution. The appearance of a blue-shifted band indicates the presence of H-aggregation. (d) Fluorescence emission and excitation spectra of the dye in EtOH and in CCl_4, showing a small aggregate contribution to the monomer fluorescence at 16 000 cm^{-1}.

transition charges method in its TrEsp (transition charge from electrostatic potential) formulation,[37] thus assessing the validity of the TrEsp method to compute exciton couplings in these aggregates.

Steady state characterization

The chemical structure of the modified ZnPc dye under investigation, originally designed as a sensitizer for DSSCs,[29] is shown in Fig. 1a. Compared to the basic ZnPc structure, the macrocycle is asymmetrically substituted with different functional moieties. We previously investigated the ultrafast behavior of the isolated chromophore in ethanol and adsorbed on titania and zirconia nanostructured films by means of transient absorption spectroscopy, obtaining evidence of H-aggregation of the dye deposited on the oxide films.[6,38]

The absorption spectrum of the dye in ethanol (Fig. 1c) shows a main spectral feature composed of two peaks, centered at 14 860 cm^{-1} and 14 580 cm^{-1}, attributed to the S_0–S_1 transition, with a vibronic progression visible at higher energies (15 700 cm^{-1} and 16 300 cm^{-1}). This band, relative to a double-degenerate state in the unperturbed parent molecule, is spitted into two components (Q-bands) due to symmetry breaking introduced by the phenyl-ethynyl group linked to the carboxylic group.[39,40]

Preliminary excited state calculations at DFT level on the monomer in different solvents are reported in Fig. S7 (ESI†), showing a good agreement with the experimental data. In particular, two transitions with similar oscillator strengths are retrieved from computations, with an energy difference on the same order of magnitude of the Q band splitting observed in the experiment (see Table ST1 in ESI†). The monomer absorption spectra show appreciable solvatochromism and a distinct behavior in nonpolar, polar and protic solvents, which are well reproduced from computations.

When the molecule is dissolved in chloroform, the absorption spectrum (Fig. 1b) clearly shows the appearance of a new broad band, blue-shifted by about 1500 cm^{-1}, which is consistent with the formation of H-type aggregates.[41,42] The aggregate absorption band is considerably broadened, indicating relaxation effects on the lineshape and the presence of conformational disorder.

Aggregation phenomena were investigated in different solvents (Fig. S9a and b, ESI†): we found that aggregation is favored in solvents with low-coordination capability, while coordinating solvents such as methanol or ethanol prevent aggregation, in agreement with previous studies.[43]

A TEM image of the sample, reported in Fig. S8 of ESI,† shows presence of aggregate structures whose size extends over several tens of nanometers, surrounded by monomers still present in the sample. To have an estimate of the monomer concentration in the presence of aggregate we performed spectral deconvolution analysis of the linear absorption spectra collected in ethanol, where only monomers are present and chloroform,

where aggregation occurs (see Fig. S9 of ESI†) This analysis suggests that monomer absorption contributes to the 26% of the total signal in presence of aggregation. A detailed description of the analysis is reported in ESI† section.

Emission and excitation spectra in different solvents are reported in Fig. 1d: even in the presence of aggregates, only the emission from the lowest electronic state of the monomer is observed, showing a small Stokes shift of about 380 cm^{-1} respect to the lowest energy absorption band. Beside a frequency shift due to solvatochromic effect, no significant difference is observed between the emission in ethanol, where only the monomer is present, and in carbon tetrachloride, where aggregation occurs, suggesting that the aggregates are not fluorescent. As observed in literature,[44–46] generally H-aggregates present very efficient non-radiative channels, so that fluorescence is strongly quenched.

Ultrafast spectroscopy of the monomer

We performed pump–probe experiments on the dye dissolved in ethanol and in diethyl ether solutions, where only the monomer is present, in order to investigate the excited state dynamics of the system and to identify the monomer contribution to the transient signal also in the presence of aggregates. The sample was excited with broadband pulses in the 13 000–16 000 cm^{-1} frequency region. The time delay between pump and probe was scanned up to 60 ps. The pump–probe 2D time-frequency maps recorded in ethanol are shown in Fig. 2a, the short timescale is highlighted in Fig. S11 of ESI.† The negative spectral features (blue color) are due ground state bleaching (GSB) and stimulated emission (SE).[6] The small positive signal between 15 000 cm^{-1} and 16 000 cm^{-1} is the low-frequency tail of the excited state absorption (ESA) that is very broad and weak,[6] inducing a small perturbation on the spectral window under investigation.

Signal decay measured at different wavelengths shows a multi exponential evolution. The recorded transient data were analyzed with a global analysis procedure using a sequential decay scheme and three kinetics components (Glotaran software).[47] The analysis provides three evolution-associated decay spectra (EADS), shown in Fig. 2b, whose lifetimes are reported in Table 1. Since the analyzed time-window is much shorter than the excited state lifetime of the dye, the long time-component is fixed to the value of 4 ns, which we previously found on the same system by transient absorption measurements performed on a more extended timescale.[6]

The transient signal shows a limited lineshape evolution, as evidenced by normalizing the EADS (see the inset of Fig. 2b). Only a small change in the intensity-ratio of the two Q-bands is observable between the two short-timescale EADS components (blue and green lines in Fig. 2b). This spectral evolution is consistent with the occurrence of an internal conversion process between the two non-degenerate Q-states.

Similar results are obtained when the measurements are repeated in diethyl ether (Fig. S10, ESI†). The system behaves

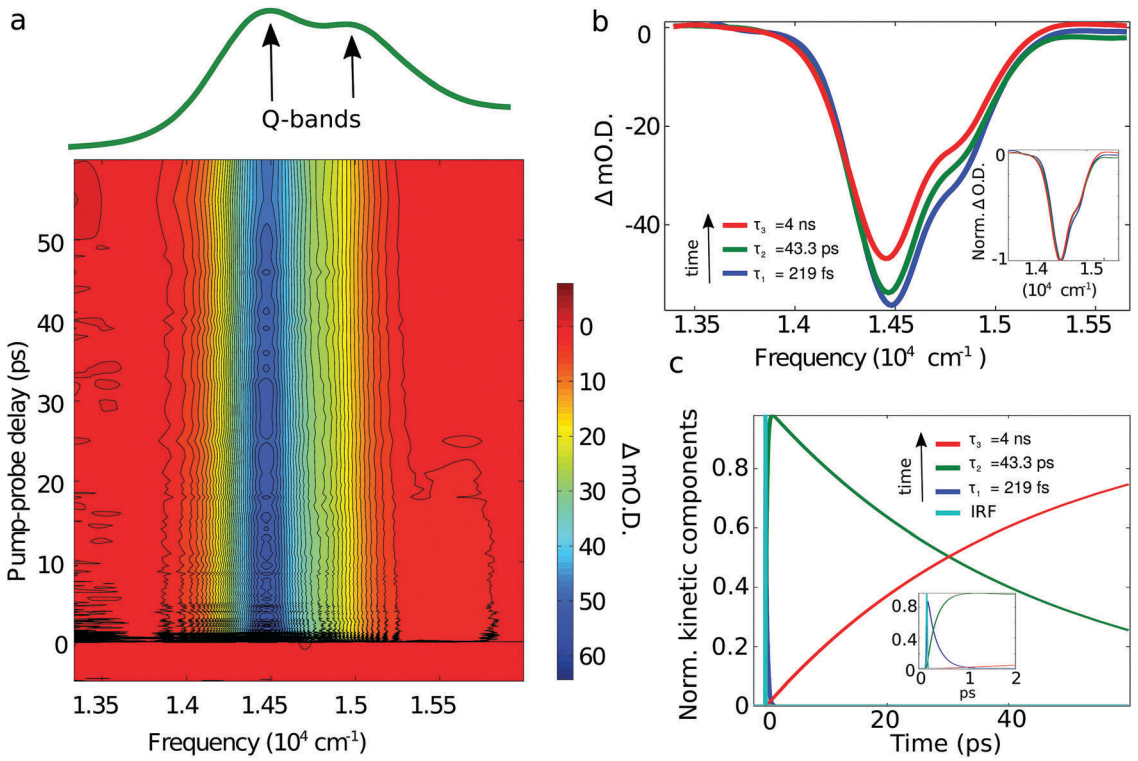

Fig. 2 (a) Broadband pump–probe 2D time–frequency map of the dye in ethanol, where only the monomer is present (linear absorption spectrum on top). (b) EADS of the transient spectra achieved by Global analysis using a sequential model involving three kinetic parameters. Normalized EADS in the inset. (c) Normalized kinetic components describing the time-evolution of the EADS anche the IRF. Zoom of the first 2 ps in the inset.

Table 1 Time constants associated to the evolution of the EADS of the ZnPc dye in different solvents: in ethanol and diethyl ether only the monomer is present in solution, while aggregation occurs in chloroform. The global analysis is performed by using a sequential model, where each transient state transfers population to the following one and finally the third and last relaxes to the ground state

Solvent	τ_1 (fs)	τ_2 (ps)	τ_3 (ns)
Ethanol	219	43.3	4
Diethylether	540	25.7	4
Chloroform	538	13.8	4

very similarly in these two solvents, showing that the electronic properties of the monomer are only slightly influenced by solvent effects, and no aggregation is involved in the excited state dynamics.

The kinetic traces corresponding to the bleaching of the ground state signal, recorded both in ethanol and in diethyl ether, show oscillations in the intensity, which last for over one picosecond. A Fourier transform analysis on these traces, reported in the ESI† (Fig. S8), shows the presence of two oscillatory components, at around 730 cm^{-1} and 760 cm^{-1}, which correspond to two ground state Raman active modes of the molecule.[48]

To have a more complete picture of the excited state dynamics of the monomer, we measured 2D electronic spectra of the system in ethanol. Fig. 3a–c report the 2D maps recorded respectively at 60, 180 and 300 fs population times τ_2; maps recorded at further delay-times are reported in ESI† (Fig. S13). Every 2DES map is normalized with respect to its own minimum and by setting the same number of colour levels. In this way, the minimum of the bleaching signal in every map corresponds to the same colour. This was done in order to obtain a better visualization of the lineshape at long times.

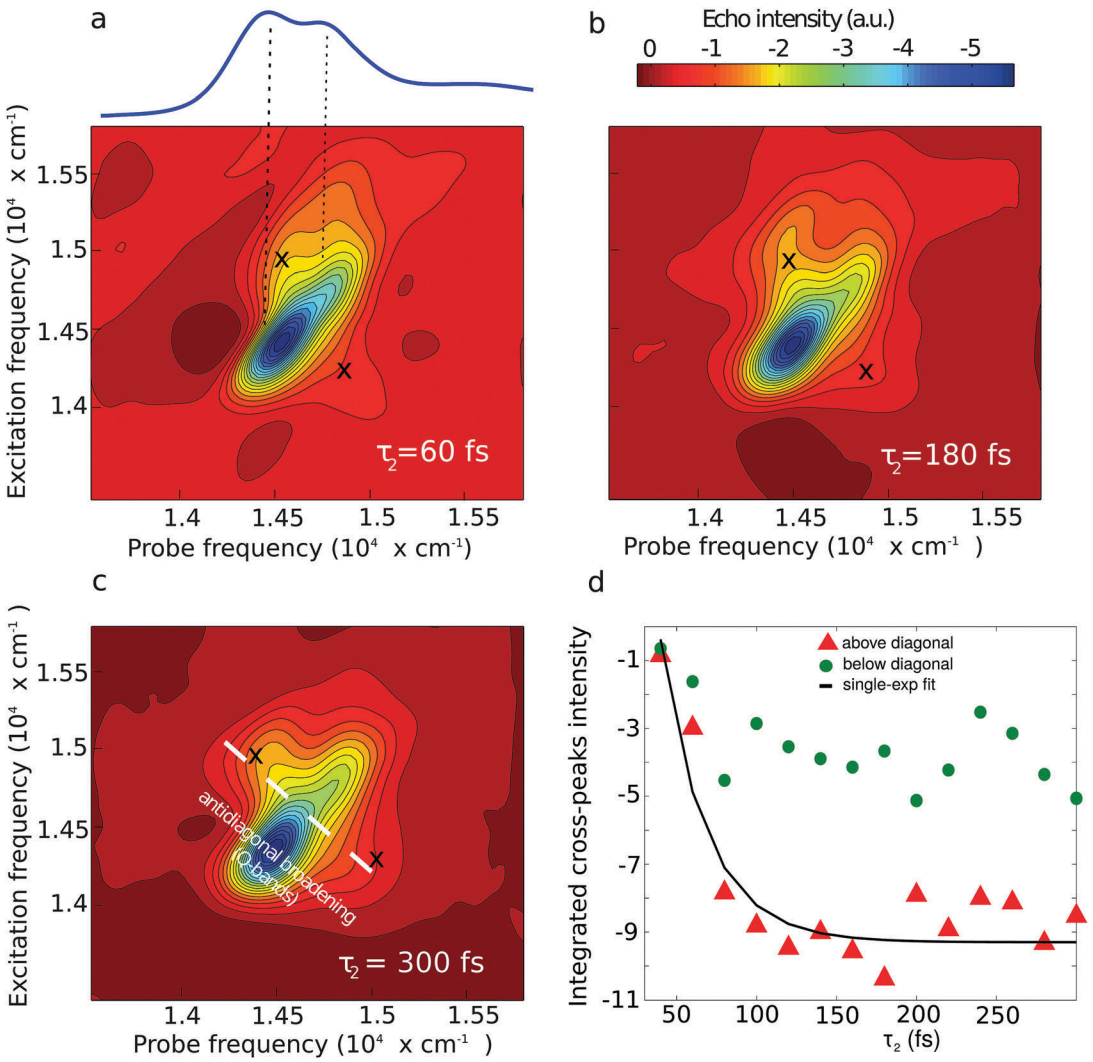

Fig. 3 Absorptive 2DES maps of ZnPc dye in EtOH at recorded 60 fs (a), 180 fs (b) and 300 fs (c). It is noticeable the growing and lineshape evolution of the cross peaks attributed to the coupling between the two Q-states and to vibronic relaxation. Furthermore, the antidiagonal broadening of the ground state bleaching component over time is indicative of spectral diffusion occurring on those timescales. (d) Integrated cross-peaks intensity as a function of τ_2, extracted from the 2DES spectra. The intensity of the cross peak above the diagonal grows with a time constant of 30 fs (single exponential fit in black), while the cross peak below the diagonal is approximatively constant in the first 300 fs.

The early time map shows an elongated diagonal peak due to the convolution of the bleaching signals of the two Q-bands of the dye, whose line-shape evolution can be followed in time.

Besides the diagonal contribution, the maps in Fig. 3 show the appearance of two cross peaks whose energy correspond to that of each Q-band, a clear indication of the presence of interaction between the two states. The antidiagonal cut of the 2D map showing the broadening of the spectral features due to the overlap with cross peaks is reported in Fig. S14 (ESI†). The stronger intensity of the peak above diagonal suggests the presence of population transfer between the Q-bands. This conclusion is in agreement with the analysis of pump–probe data, evidencing a change in the intensity ratio of the bleaching signals due to the two Q states on a two-hundred femtoseconds timescale (inset of Fig. 2b). The kinetics of the above-diagonal cross peak shows a clear time-evolution, with a rise constant of about 30 fs, ascribable to the thermal relaxation within the excited state.

Due to the very small energy difference between the Q-bands, the cross-peaks overlap the diagonal bleaching component, resulting in an overall weak antidiagonal broadening. This overlap is minimized in diethyl ether, where diagonal and off-diagonal contributions can be clearly distinguished (see Fig. S16 in ESI†).

2D electronic spectra provide a measure of the frequency-fluctuation correlation function (FFCF).[46,50] The decay of the FFCF as a function of τ_2 describes the time evolution of the transition frequencies distribution, determined by static and dynamic disorder.[50,51]

The maps reported in Fig. 3a–c, show antidiagonal broadening of the signal at increasing τ_2, concomitant with a reduction of the diagonal linewidth. This evolution indicates that spectral diffusion occurs on timescales of hundred of femtoseconds: the system is going through all the static configurations determined by its inhomogeneity, relaxing toward the homogeneous limit.[52,53] We have to remind that lineshape evolution due to the interaction of the two Q states also occurs on this same timescale.

Several measures of the FFCF have been proposed in the literature to study the time evolution of the lineshape in 2DES spectra.[54–57] Among them, Lazonder and Tokmakoff[53,58] demonstrated the equivalence between the FFCF and the ellipticity e of a 2D spectral feature, defined as

$$e = \frac{D^2 - A^2}{D^2 + A^2} \quad (1)$$

where A and D are the antidiagonal and diagonal full width at half maximum (FWHM), respectively. We used this method to estimate the timescale of spectral diffusion in the ZnPc system. Since the model underlying eqn (1) is applicable to a single transition, the ellipticity was estimated only for the most intense, low-energy transition (centered at 14 500 cm^{-1}). Fig. 4a and b respectively report diagonal and antidiagonal slices extracted from the 2DES spectra as a function of population time τ_2. The diagonal slices are inhomogeneously broadened, and represent the convolution of the two Q-bands. We deconvolved the Gaussian features associated to each transition in order to extract the FWHM of the low-energy band (details in the ESI,† see Fig. S15) and used this value as factor D in eqn (1). The antidiagonal lineshape consists of two contributions: homogeneous broadening and splitting of the Q-states. In order to avoid the contribution of the cross-peaks, the antidiagonal slices are taken at the frequency corresponding to the low-energy Q-state, around 14 500 cm^{-1}.

Fig. 4c reports the ellipticity, evaluated for the low-energy Q-band, as a function of τ_2 (red dots), on top of a mono-exponential decay fit (black curve), retrieving a time constant for the spectral diffusion of 344 fs. Such a long relaxation time includes both solvent effects and internal conversion between Q-states, and it is in agreement with previous studies on similar light-harvesting chromophores, such as porphyrins.[49,59]

Ultrafast spectroscopy of the aggregate

A pump–probe 2D-plot of the dye in chloroform, where aggregation occurs, is presented in Fig. 5. Data were analyzed with the same global analysis procedure previously described. The three EADS are reported in Fig. 5b and the time-constants of the three kinetics components in different solvents are reported in Table 1. The sample shows a very different behavior compared

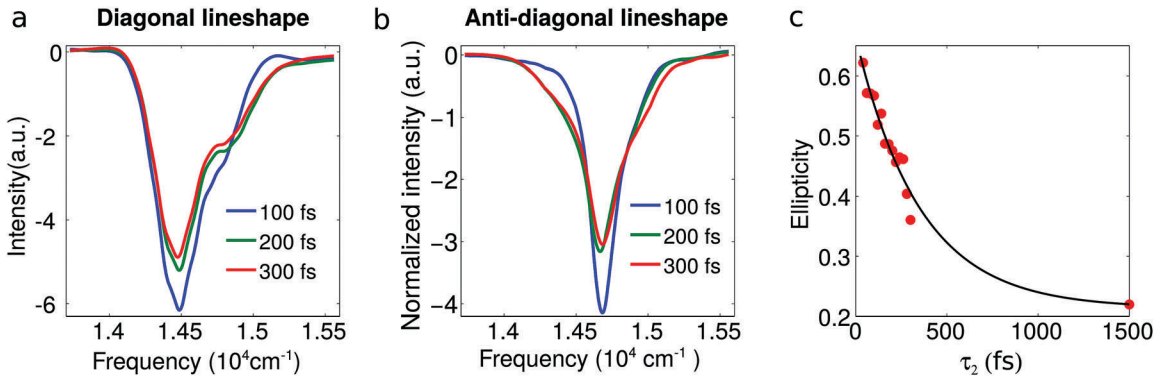

Fig. 4 Diagonal (a) and antidiagonal (b) lineshape extracted from 2DES maps recorded at different population time τ_2. In order to extract diagonal and antidiagonal linewidth relative to the low energy band, we deconvolved the diagonal spectra with two Gaussian components (see ESI†). The Lorentzian lineshape of the antidiagonal spectra is evident, meaning that off-diagonal contribution due to cross-peaks are negligible. (c) Ellipticity (defined in eqn (1)) as a function of population time on top of mono-exponential fit. A spectral diffusion time constant of 344 fs was found.

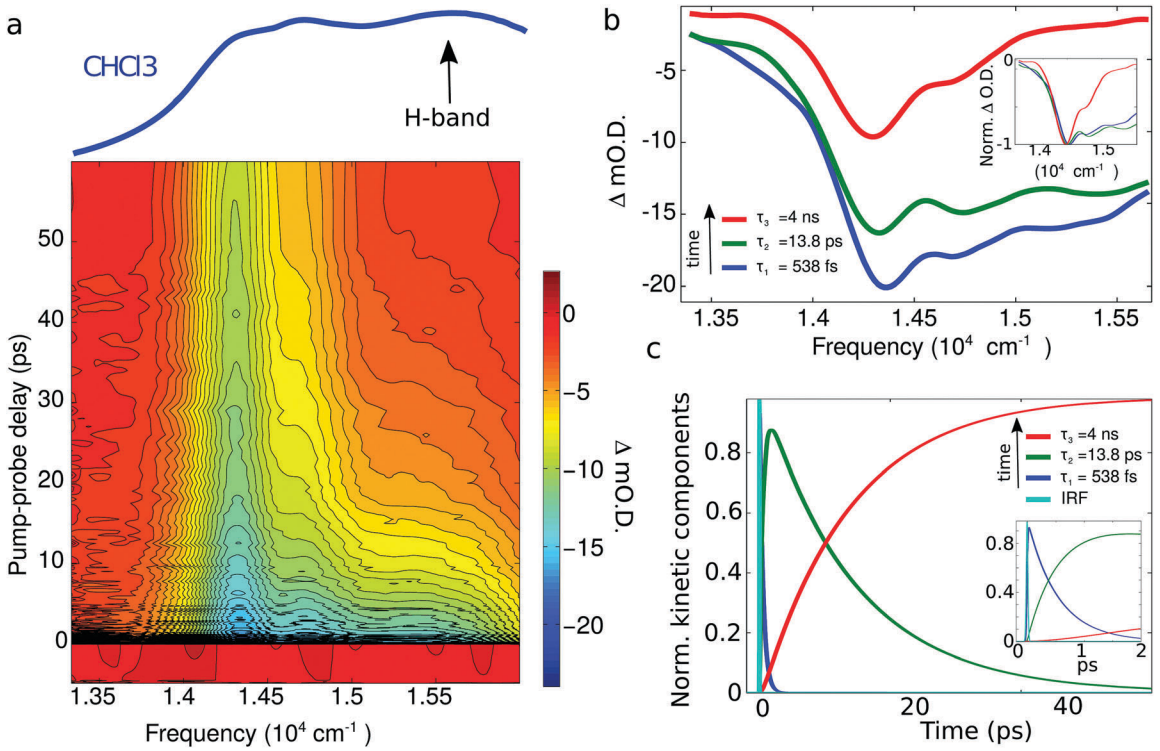

Fig. 5 (a) Broadband pump–probe 2D time–frequency map of the dye in $CHCl_3$, where aggregation occurs (linear absorption spectrum on top). (b) EADS retrieved by Global analysis using a sequential model involving three kinetic components. Normalized EADS in the inset. (c) Normalized kinetic components describing the time-evolution of the EADS. Zoom of the first 2 ps in the inset.

to what observed in ethanol. In chloroform we observe an ultrafast time component (538 fs) resulting in a change in the relative intensity of the low and high frequency side of the overall broad negative band between the first two EADS (see the inset of Fig. 5b). This evolution is ascribable to the relaxation of the aggregate state populated immediately after excitation towards lower energy states. The intermediate time constant of 13.8 ps is mainly associated with a substantial decay of the aggregate signal. The long-lasting spectral component, decaying in 4 ns, reflects the signal due to residual monomers, which, on the long timescale follow their intrinsic dynamics. In fact, the third EADS in Fig. 5 essentially coincides with the analogous one in Fig. 2, besides differences in the lineshape and shift of peak position due to the different solvent.

We performed a spectral deconvolution analysis on the EADS, in order to quantify the monomer contribution to the transient signal (Fig. S17 of ESI†). We found that the area of the fitting curve of the long-lasting EADS, which reflects the residual monomers, is 24% of the initial one, which is in very good agreement with the deconvolution analysis of the linear absorption spectra (Fig. S9 of ESI†). Detailed description of the analysis is reported in ESI† section.

In order to further disentangle the monomer and aggregate contributions in the transient signal, we plot in Fig. 6 the kinetic traces of the monomer GSB in different solvents and that of the aggregate GSB in chloroform, superimposed to the exponential decay fits retrieved from global analysis (black lines). In case of chloroform, monomer and aggregate contributions

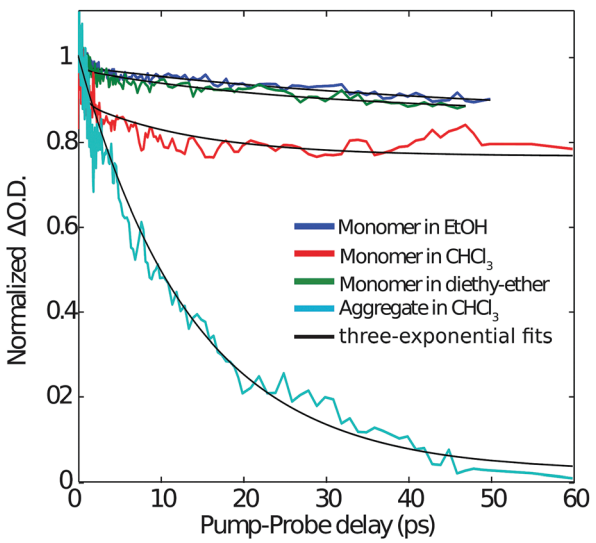

Fig. 6 Normalized decay kinetics from pump–probe data showing different behaviour between monomers in ethanol (from pump–probe data in Fig. 2) and in diethyl-ether (from pump–probe data in Fig. S10, ESI†), and aggregates and monomers chloroform (from pump–probe data in Fig. 5). The black curves are three-exponential fits with time-constants taken from global analysis. The kinetics in $CHCl_3$ are obtained by a double-Voigt deconvolution of the spectra as a function of time. The plotted kinetics are the integrated area under the two Voigt curves, representing the monomer bleaching band and the aggregate absorption band respectively. Monomers dynamics are influenced by the presence of aggregates, resulting in a faster decay.

have been deconvolved by fitting the spectra at each delay time with two Voigt components, centered at the transition frequencies of monomer and aggregate (14 400 cm^{-1} and 15 500 cm^{-1} respectively). The reported traces (red and cyan lines in Fig. 6) are obtained by plotting the integrated area under the two Voigt functions as a function of pump–probe delay. The small difference between the monomer recovery in ethanol and in diethyl ether (full pump–probe 2D map in Fig. S10, ESI†) is attributed to a solvent effect, and in particular to the larger spectral separation of the two Q transitions observed in diethyl ether. On the other hand, a strong influence of the aggregate on the tens of picosecond timescale can be noticed by comparing the trace taken in the monomer region in chloroform with those of the two other solvents: the recovery is much faster in chloroform than in methanol or diethyl ether, where aggregation does not occur. This is ascribable to the fact that the aggregate band extends far in the red, as shown in the deconvolution analysis reported in Fig. S9 (ESI†), causing an overall speeding up of the recovery process. In addition, while the monomer kinetics is dominated by a long time-component, the aggregate is completely relaxed after 60 ps, in agreement with the global analysis results shown above.

The fast decay of the aggregate signal results from multiple reasons. Besides the occurrence of fast non-radiative decay due to exciton coupling, exciton–exciton annihilation (EEA) can also play a role. EEA is a phenomenon commonly observed in excitonic systems even at low excitation powers. We haven't carried out any power dependent measurements to quantify the amount of EEA, but we cannot exclude its effect on the observed kinetic behaviour.

The oscillations previously described for the GSB traces in ethanol are only slightly visible in the presence of the aggregates, probably because now structural disorder broadens the absorption features, preventing a full coherent excitation of the vibrational modes. The pump–probe data in chloroform are consistent with the presence of both monomers and aggregates in solution, in agreement with TEM images (shown in Fig. S8, ESI†). In order to further investigate the dynamics of such a complex mixture, we carried out coherent 2D spectroscopy on the system.

2DES maps recorded at a population time τ_2 of 200 fs and in different aggregation conditions in chloroform are reported in Fig. 7. The linear absorption spectrum is reported on the right side of the 2D maps, showing a higher amount of aggregate formation in panel b, which refer to a more concentrated solution. Both maps reported in Fig. 7a and b clearly show the diagonal contribution of the aggregate response in the high-energy region (around 15 500 cm^{-1}).

The aggregate feature in Fig. 7a is broadened below the diagonal due to excitonic coupling, as observed previous work.[60]

In the situation of high aggregate concentration, Fig. 7b (> 5 mM), three main peaks are evident: two along the diagonal and one above the diagonal. The diagonal peak located at 14 400 cm^{-1} is related to the monomer signal, while the elongated peak around 15 500 cm^{-1} represents the signal from the aggregate.

The aggregate peak is located slightly off the diagonal, similarly to what previously observed in the 2D spectra of other interacting multichromophoric system or in condensed phase.[60–62] This shift has been attributed to the presence of strong excitonic coupling. An additional phenomenon possibly contributing to the observed spectral shape is the superposition between a positive ESA and negative signal (GSB + SE). In a previous transient absorption study[6] we reported indeed that the ESA intensity, which is very poor in the monomer solution, appears to be strongly dependent on the aggregation degree.

The above diagonal peak related to the interaction of the Q-states is scarcely visible in Fig. 7b, due its overlap with the broad excitonic peak, while the one below diagonal is still visible, although its intensity is lowered due to overlap with the ESA contribution.

The frequency position of the most intense cross-peak in Fig. 7b (at 14 600, 15 400) cm^{-1} doesn't point to a direct interaction

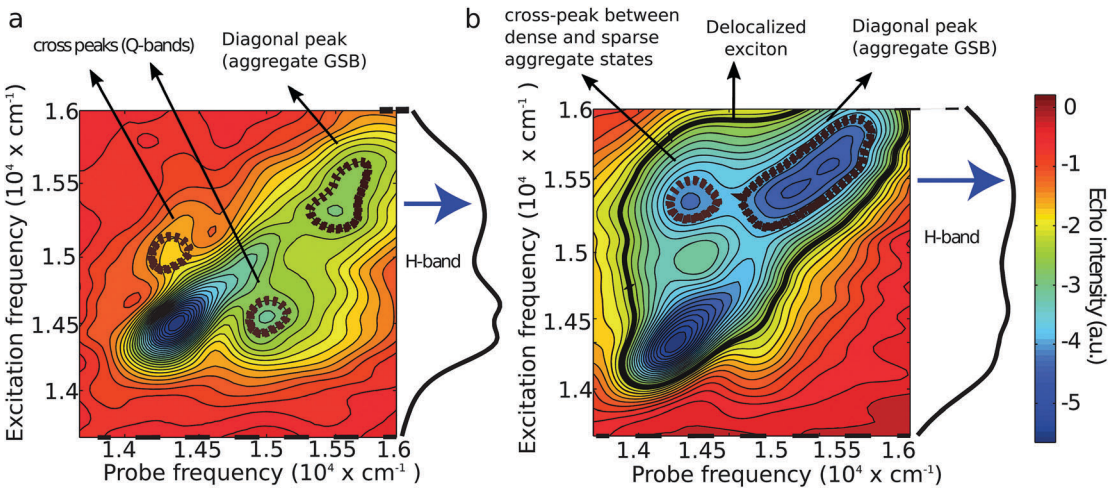

Fig. 7 2DES maps recorded at τ_2 = 200 fs of the dye in $CHCl_3$ at low aggregate concentration (a) and high aggregate concentration (b). The black curves on the right are the absorption spectra of the two samples. The cross peaks in (a) are attributed to the Q-states coupling. The cross peak in map (b) is attributed to an electronic coupling established between 'sparse' and 'dense' aggregates.

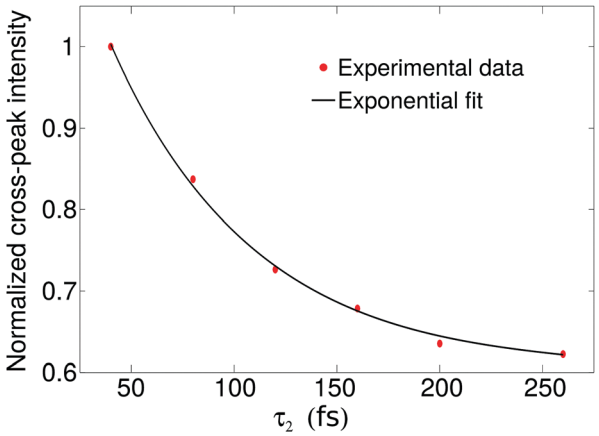

Fig. 8 Normalized cross-peaks intensity as a function of τ_2 (violet dots) extracted from the 2DES spectra in Fig. S19 (ESI†) (case of high aggregate concentration). The blue line is the single-exponential fit.

between monomers and aggregates, but rather to a coupling among exciton states, which reflects the conformational disorder of the aggregates, due both to different aggregate dimensions and to a different degree of interaction among monomers.

The wide 2D spectral shape indeed suggests the presence of a distribution of intermediate structures going from monomer to extended aggregates, implying the occurrence of a distribution of transition energies among which the exciton can spread over.

This gives rise to an energy flow from the exciton states in which monomers are more strongly coupled (''dense aggregate states'') to peripheral molecules, which are less interacting with the dense core of the aggregate (''sparse aggregate states''). The ''dense aggregate states'' thus represent strongly packed monomers, whose energetic levels and relaxation pathways are considerably perturbed by the intermolecular interactions, resulting in a blue-shifted non-linear response. When these H-states are excited, energy flows toward the periphery, where the electronic properties are much more similar to those of isolated monomers, whose spectral response is more shifted toward the red side of the frequency window.

In order to have a qualitative information about the aggregate dimension we fitted the linear absorption spectra in the presence of aggregate using a simple exciton model based on a Frenkel Hamiltonian (see Fig. S20 of ESI†). The results of this simplified analysis show that a satisfactory fit can only be obtained by introducing both static and dynamic disorder, thus supporting the idea that aggregates of different size and with a distribution of coupling strengths among the molecular units composing the aggregate are present in solution.

The 2DES spectra recorded at different population time in the two cases (low and high aggregate concentration) are reported in Fig. S18 and S19 respectively (see ESI†). The dynamics of energy flow among different exciton states of the aggregate can be inferred by plotting the integrated intensity of the cross peak observed at 15 400 cm^{-1} excitation frequency and 14 600 cm^{-1} probe frequency, showing a decay component of about 70 fs (Fig. 8).

Conclusions

The complex exciton dynamics of a disordered H-aggregate of substituted ZnPc molecule has been investigated by combining stationary and time-resolved spectroscopy, TEM, quantum chemistry calculations and Frenkel exciton modeling. We have characterized the aggregation behavior of the dye in solution at various concentration and in different solvents. Broadband pump–probe and 2D-ES spectroscopy were applied to compare the excited state relaxation between monomer and aggregates. In solvents where only the monomer is present an ultrafast internal conversion among the non-degenerate Q states is evidenced by the appearance of a cross peak. We furthermore show that in solvents where aggregates form, the dynamics of the system is more complicated and highly influenced by the concentration. In particular, the analysis of the 2D maps of solutions with high aggregate concentration shows the appearance of a cross peak, which we attribute to the interactions among aggregates of different size, which we term 'dense' and 'sparse' aggregate states. The kinetic of the cross peak evidences that the timescale of exciton relaxation within a distribution of transition energies of the aggregate ranges on a <100 fs timescale.

Conflicts of interest

There are no conflicts to declare.

Acknowledgements

This project has received funding from the European Union's Horizon 2020 research and innovation programme under grant agreement no. 654148 Laserlab-Europe, (Short: Laserlab-Europe, H2020 EC-GA 654148).

References

1 B. J. A. A. W. Elemans, R. Van Hameren, R. J. M. Nolte and A. E. Rowan, *Adv. Mater.*, 2006, 1251–1266.
2 G. de la Torre, C. G. Claessens and T. Torres, *Chem. Commun.*, 2007, 2000–2015.
3 J. C. Bommer and J. D. Spikes, *Photochem. Photobiol.*, 1991, **53**(3), 419.
4 M. C. Feiters, M. C. T. Fyfe, M. V. Martinez-Diaz, S. Menzer, R. J. M. Nolte, J. F. Stoddart, P. J. M. Van Kan and D. J. Williams, *J. Am. Chem. Soc.*, 1997, **119**(34), 8119–8120.
5 H. Ali and J. E. Van Lier, *Chem. Rev.*, 1999, **99**, 2379–2450.
6 A. Iagatti, S. Doria, A. Marcelli, N. Angelini, S. Notarantonio, A. M. Paoletti, G. Pennesi, G. Rossi, G. Zanotti, G. Calogero and P. Foggi, *J. Phys. Chem. C*, 2015, **119**(35), 20256–20264.
7 C. G. Claessens, U. Hahn and T. Torres, *Chem. Rec.*, 2008, **8**(2), 75–97.
8 M. Ince, J. H. Yum, Y. Kim, S. Mathew, M. Grätzel, T. Torres and M. K. Nazeeruddin, *J. Phys. Chem. C*, 2014, **118**(30), 17166–17170.

9 M. V. Martínez-Díaz, G. de la Torre and T. Torres, *Chem. Commun.*, 2010, **46**(38), 7090–7108.
10 R. Šilerová, L. Kalvoda, D. Neher, A. Ferencz, J. Wu and G. Wegner, *Chem. Mater.*, 1998, **10**(8), 2284–2292.
11 G. de la Torre, P. Vàzquez, F. Agullò-Lòpez and T. Torres, *Chem. Rev.*, 2004, **104**, 3723–3750.
12 G. da la Torre, P. Vazquez, F. Agullò-Lòpez and T. Torres, *J. Mater. Chem.*, 1998, **8**(8), 1671–1683.
13 S. M. Bishop, A. Beeby, A. W. Parker, M. S. C. Foley and D. Phillips, *J. Photochem. Photobiol., A*, 1995, **90**(1), 39–44.
14 A. Beeby, S. Fitzgerald and C. F. Stanley, *J. Chem. Soc., Perkin Trans. 2*, 2001, 1978–1982.
15 J. R. D. P. Douglas, A. H. G. Porter and M.-C. Richoux, *Coord. Chem. Rev.*, 1982, **44**, 83–126.
16 J. R. Gray and H. B. Winkler, *The Porphyrin Handbook, Bioinorganic and Bioorganic Chemistry*, 2003.
17 K. M. Kadish, K. M. Smith and R. Guilard, *The porphyrin handbook, Applications of phthalocyanines*, Academic Press, 2003, vol. 19.
18 R. Bonnett, *Chem. Soc. Rev.*, 1995, **24**(1), 19.
19 A. E. O'Connor, W. M. Gallagher and A. T. Byrne, *Photochem. Photobiol.*, 2009, **85**(5), 1053–1074.
20 N. Kobayashi, M. Togashi, T. Osa, K. Ishii, S. Yamauchi and H. Hino, *J. Am. Chem. Soc.*, 1996, **118**(5), 1073–1085.
21 I. RuUckmann, A. Zeug, R. Herter and B. Roder, *Photochem. Photobiol.*, 1997, **66**(5), 576–584.
22 L. Howe and J. Z. Zhang, *J. Phys. Chem. A*, 1997, **101**(18), 3207–3213.
23 P. G. Schouten, J. M. Warman, M. P. De Haas, C. F. van Nostrum, G. H. Gelinik, R. J. M. Nolte, M. J. Copyn, J. W. Zwikker, M. K. Engel, M. Hanak, Y. H. Chang and W. T. Ford, *J. Am. Chem. Soc.*, 1994, **116**, 6880–6894.
24 P. Smolenyak, R. Peterson, K. Nebesny, M. Torker, D. F. O'Brien and N. R. Armstrong, *J. Am. Chem. Soc.*, 1999, **121**(15), 8628–8636.
25 H. Abramczyk and I. Szymczyk, *J. Mol. Liq.*, 2004, **110**(1–3), 51–56.
26 H. Abramczyk, B. Brozek-Płuska, K. Kurczewski, M. Kurczewska, I. Szymczyk, P. Krzyczmonik, T. Błaszczyk, H. Scholl and W. Czajkowski, *J. Phys. Chem. A*, 2006, **110**(28), 8627–8636.
27 A. Laschewsky, *Angew. Chem.*, 1989, **28**(11), 1574–1577.
28 M. J. Cook, B. M. John, M. S. Andrew, M. F. Daniel, K. J. Harrison, R. M. Richardson and S. J. Roser, *J. Mater. Chem.*, 1991, **1**, 121–127.
29 G. Zanotti, N. Angelini, A. M. Paoletti, G. Pennesi, G. Rossi, A. A. Bonapasta, G. Mattioli, A. Di Carlo, T. M. Brown, A. Lembo and A. Reale, *Dalton Trans.*, 2011, **40**, 38–40.
30 J. R. Caram, S. Doria, D. M. D. M. Eisele, F. S. Freyria, T. S. Sinclair, P. Rebentrost, S. Lloyd and M. G. Bawendi, *ACS Nano*, 2016, **16**(11), 6808–6815.
31 S. Doria, T. S. Sinclair, N. D. Klein, D. I. G. Bennett, C. Chuang, F. S. Freyria, C. P. Steiner, P. Foggi, K. A. Nelson, J. Cao, A. Aspuru-Guzik, S. Lloyd, J. R. Caram and M. G. Bawendi, *ACS Nano*, 2018, **12**, 4556–4564.
32 N. Azzaroli, *Optical set-up development and software interface of 2D-visible coherent spectroscopy experiment to investigate dynamics of multi-chromophoric molecular complexes*, University of Florence, Italy, 2015.
33 Y. Zhao and D. G. Truhlar, *Theor. Chem. Acc.*, 2008, **120**(1–3), 215–241.
34 J. Tomasi, B. Mennucci and R. Cammi, *Chem. Rev.*, 2005, **105**, 2999–3093.
35 S. Grimme, J. Antony, S. Ehrlich and H. Krieg, *J. Chem. Phys.*, 2010, **132**, 15.
36 C. P. Hsu, G. R. Fleming, M. Head-Gordon and T. Head-Gordon, *J. Chem. Phys.*, 2001, **114**(7), 3065–3072.
37 M. E. Madjet, A. Abdurahman and T. Renger, *J. Phys. Chem. B*, 2006, **110**(34), 17268–17281.
38 G. Pellegrino, A. Alberti, G. G. Condorelli, F. Giannazzo, A. La Magna, A. M. Paoletti, G. Pennesi, G. Rossi and G. Zanotti, *J. Phys. Chem. C*, 2013, **117**, 11176–11185.
39 M. S. Liao and S. Scheiner, *J. Chem. Phys.*, 2001, **114**(22), 9780–9791.
40 K. A. Nguyen and R. Pachter, *J. Chem. Phys.*, 2003, **118**(13), 5802–5810.
41 J. L. Herek and A. Huijser, *J. Phys. Chem. C*, 2013, **117**, 25397–25404.
42 O. E. Sielcken, M. M. Van Tilborg, M. F. M. Roks, R. Hendriks, W. Drenth and R. J. M. Nolte, *J. Am. Chem. Soc.*, 1987, **109**(14), 4261–4265.
43 E. T. Saka, C. Göl, M. Durmus, H. Kantekin and Z. Bıyıklıo, *J. Photochem. Photobiol., A*, 2012, **241**, 67–78.
44 M. Kasha, H. R. Rawls and M. Ashraf El-Bayoumi, *Pure Appl. Chem.*, 1965, **11**, 371–392.
45 F. C. Spano, *Acc. Chem. Res.*, 2009, **43**(9), 429–439.
46 M. Wang, G. L. Silva and B. A. Armitage, *J. Am. Chem. Soc.*, 2000, **122**, 9977–9986.
47 J. J. Snellenburg, S. P. Laptenok, R. Seger, K. M. Mullen and I. H. M. van Stokkum, *J. Stat. Softw.*, 2012, **49**, 3.
48 D. R. Tackley, D. Geoffrey and W. E. Smith, *Phys. Chem. Chem. Phys.*, 2001, **3**, 1419–1426.
49 K. L. Wells, Z. Zhang, J. R. Rouxel and H.-S. Tan, *J. Phys. Chem. B*, 2013, **117**(8), 2294–2299.
50 M. Khalil, N. Demirdoven and A. Tokmakoff, *J. Phys. Chem. A*, 2003, **107**(27), 5258–5279.
51 T. Brixner, T. Mančal, I. V. Stiopkin and G. R. Fleming, *J. Chem. Phys.*, 2004, **121**(9), 4221–4236.
52 P. Hamm and M. Zanni, *Concepts and Methods of 2D Infrared Spectroscopy*, Cambridge, 2011, vol. 28, p. 3.
53 S. T. Roberts, J. J. Loparo and A. Tokmakoff, *J. Chem. Phys.*, 2006, **125**, 8.
54 K. Kwac and M. Cho, *J. Phys. Chem. A*, 2003, **107**(31), 5903–5912.
55 J. D. Hybl, A. Yu, D. A. Farrow and D. M. Jonas, *J. Phys. Chem. A*, 2002, **106**, 7651–7654.
56 N. Demirdöven, M. Khalil and A. Tokmakoff, *Phys. Rev. Lett.*, 2002, **89**(23), 237401.

57 J. R. Caram, H. Zheng, P. D. Dahlberg, B. S. Rolczynski, G. B. Griffin, D. S. Dolzhnikov, D. V. Talapin and G. S. Engel, *J. Chem. Phys.*, 2014, **140**, 84701.
58 K. Lazonder, M. S. Pshenichnikov and D. A. Wiersma, *Opt. Lett.*, 2006, **31**(22), 3354–3356.
59 R. Moca, S. R. Meech and I. A. Heisler, *J. Phys. Chem. B*, 2015, **119**(27), 8623–8630.
60 K. H. Song, M. Gu, M. S. Kim, H. J. Kwon, H. Rhee, H. Han and M. Cho, *J. Phys. Chem. Lett.*, 2015, **6**(21), 4314–4318.
61 N. S. Ginsberg, Y.-C. Cheng and G. R. Fleming, *Acc. Chem. Res.*, 2009, **42**(9), 1352–1363.
62 J. C. Dean and G. D. Scholes, *Acc. Chem. Res.*, 2017, **50**, 2746–2755.